






Charge correlations and their photoinduced dynamics in charge-ordered organic ferroelectrics

Hirotake Itoh ^{1,*}, Hirokazu Obatake,¹ Rina Fujiwara,¹ Yohei Kawakami ¹, Kaoru Yamamoto ²,
Martin Dressel ³ and Shinichiro Iwai ^{1,†}

¹Department of Physics, Tohoku University, Sendai 980-8578, Japan

²Department of Applied Physics, Okayama University of Science, Okayama 700-0005, Japan

³1. Physikalisches Institut, Universität Stuttgart, 70569 Stuttgart, Germany



(Received 22 October 2020; revised 10 May 2021; accepted 8 July 2021; published 13 August 2021)

By employing THz absorption and emission spectroscopy we were able to disentangle long-range charge order with a hundreds micrometer scale and short-range charge fluctuations that occur well above the charge-order phase transition in quasi-one-dimensional organic ferroelectrics, (TMTTF)₂X ($X = \text{AsF}_6, \text{PF}_6, \text{and SbF}_6$). While long-range charge order melts by photoexcitation irrespective of temperature or chemical pressure, short-range fluctuations are actually enhanced close to the charge-order phase boundary for $X = \text{AsF}_6$ and PF_6 . Our findings reveal that short-range fluctuations show various photoresponses depending on both temperature and electronic parameters, providing a design strategy for nonequilibrium states.

DOI: [10.1103/PhysRevResearch.3.L032043](https://doi.org/10.1103/PhysRevResearch.3.L032043)

Short-range electronic correlations have been the key issue in condensed-matter physics for decades [1,2]. They often spontaneously emerge as spatially inhomogeneous domains with nanometer-scale structures around boundaries between competing electronic phases in strongly correlated systems [3,4], triggering exotic aspects of high-temperature superconductivity [5] or colossal magnetoresistance [6]. Sometimes the short-range correlations themselves govern the electronic state of solids in the absence of long-range order, showing unique properties such as relaxor ferroelectricity, spin/dipole liquid, or charge glass, which are presently the subjects of intensive discussions [7–11].

Particularly intriguing is the role in photoinduced phase transitions [12–14]. The short-range correlations or fluctuations not only govern their ultrafast dynamics [15,16], but also become precursors from where macroscopic metallic states grow, when introduced into a charge-order (CO) background [17–19]. Moreover, a photoinduced enhancement of them was recently found to be feasible exploiting the instability around the phase boundary [20] or the strong light-field effect [21,22]. Such versatile short-range dynamics offers a promising pathway to tailor nonequilibrium photoinduced states which might be thermodynamically inaccessible [23–26]. To this end time-resolved experiments are now actively conducted to directly uncover microscopic dynamics [27–30].

Quarter-filled organic conductors (TMTTF)₂X (TMTTF: tetramethyl-tetrathiafulvalene; X: anion) [Fig. 1(a)] offer an

ideal platform for the research for their competing nature of electronic phases [31,32]. The dynamics of correlated charges can be studied as a function of both temperature and chemical substitution of X, which can tune electronic parameters via a chemical pressure effect. Therein electronic ferroelectricity is peculiarly induced by macroscopic CO below the transition temperature T_{CO} [33–36].

In this Letter, we report the charge dynamics in (TMTTF)₂X investigated by terahertz (THz) spectroscopy. Short- and long-range charge correlations were distinctively observed via THz absorption and emission measurements, respectively [Fig. 1(b)]; intermolecular vibration and macroscopic polarization were measured. The short-range correlations, which survive even above T_{CO} , exhibit a photoinduced enhancement close to the CO phase boundary for $X = \text{AsF}_6$ and PF_6 ; its amount depends on temperature. In contrast, the long-range CO shows a photoinduced suppression irrespective of temperature or X. Distinct responses indicate that charge fluctuations play the key role in photoinduced charge dynamics.

Hereafter we abbreviate TMTTF as TM. TM₂SbF₆, TM₂AsF₆, and TM₂PF₆ were synthesized by the electrochemical method [31,37]. Bulk single crystals with triclinic symmetry [38–41] having typical sizes of $2 \times 1 \times 0.1 \text{ mm}^3$ (*ab* plane) were mounted on copper plates and placed in an He exchange gas cryostat (Oxford Optistat-CF). As shown in Fig. 1(a), TM dimers stack along the *a* axis (conducting axis). Below T_{CO} , each dimer undergoes charge disproportionation due to a strong Coulomb repulsion to have (TM)^{+0.5+ δ} and (TM)^{+0.5- δ} ($2\delta \sim 0.2$ [32]). Consequent local electric dipoles form long-range order or macroscopic *P* (electronic ferroelectricity), which will be inverted upon interchanging charge-rich/charge-poor sites.

We performed two kinds of THz measurements as shown in Fig. 1(b): THz absorption (transmission), and THz emission triggered by 1.55-eV femtosecond pulses, reflecting

*hiroito@tohoku.ac.jp

†s-iwai@tohoku.ac.jp

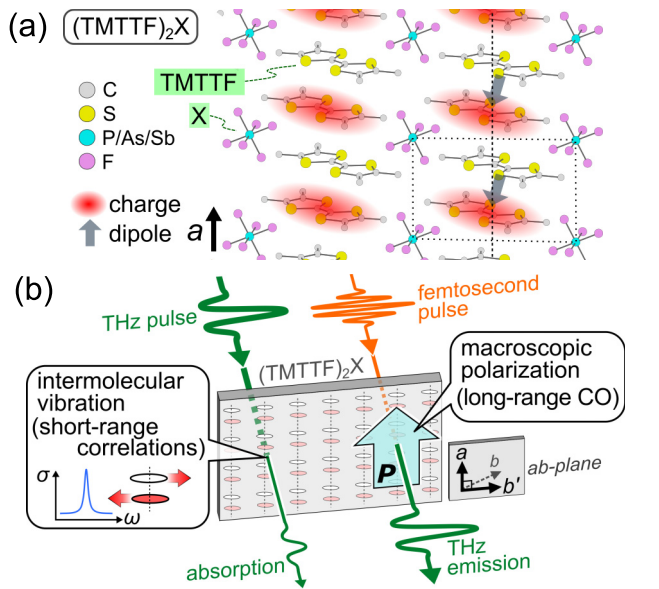


FIG. 1. (a) Schematic of TM_2X crystal (data taken from Ref. [42]), with CO and an expected electric dipole (gray arrows). The projected unit cell and stacking direction of TMTTF molecules ($\parallel a$) is indicated by dotted and dashed lines, respectively. (b) Schematics of THz absorption (left) and THz emission (right) experiments. The THz polarization ($\parallel b'$) is perpendicular to the stack; b' denotes the projection of the b axis perpendicular to the a axis, in the ab plane.

intradimer charge disproportionation and macroscopic polarization, respectively, allowing us to selectively discuss short- and long-range charge correlations. The polarization of the light was parallel to the b' axis (perpendicular to the stack [Fig. 1(b)]). The time-domain waveform of the THz electric field was collected by electro-optic sampling (time-domain spectroscopy). The experimental details are given in the Supplemental Material [43].

Figure 2(a) shows the steady-state absorption (optical density, OD) spectra of TM_2AsF_6 ; the same data are shown in the waterfall and image plot. Here, we concentrate on a peak at $\sim 66 \text{ cm}^{-1}$ which developed with decreasing temperature down to below $T_{\text{CO}} = 102 \text{ K}$. This mode has been assigned to a vibration between a pair of TM molecules having an antiphase translation along the longitudinal direction (T_c mode [32]), which becomes infrared active by charge disproportionation yielding intradimer electric dipoles [Fig. 1(a)]. Hence its oscillator strength is a measure of how short-range charge correlations develop, as will be shown later. Based on this assignment, we will refer to this peak as the SR (short-range) peak.

Figure 2(b) shows optical conductivity spectra for all compounds. Again, the SR peak of TM_2AsF_6 at $\sim 66 \text{ cm}^{-1}$ (triangle) develops with decreasing temperature from above T_{CO} . At a low temperature $T = 20 \text{ K}$, other peaks are also seen at 54, 75, and 85 cm^{-1} , in agreement with the previous study [32], where 54- and 85- cm^{-1} peaks represent T_a and T_b mode

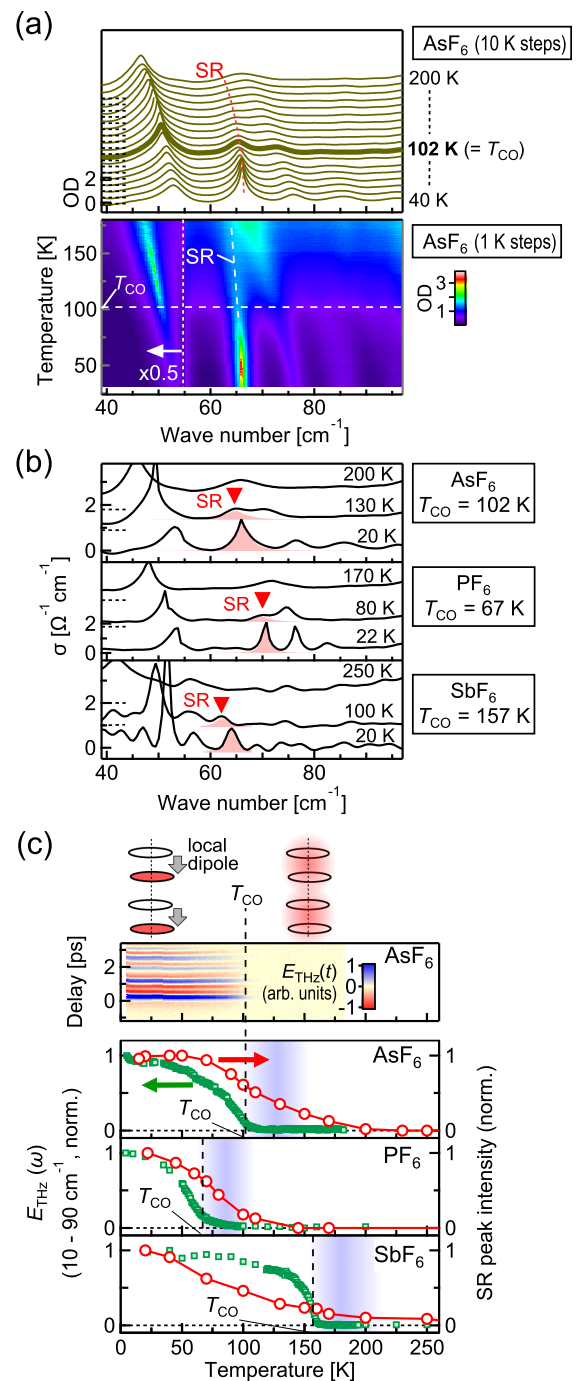


FIG. 2. (a) Absorption spectra of TM_2AsF_6 . The same data, measured in 1-K steps, are shown every 10 K (except for T_{CO}) in the upper panel, whereas they are shown in the image plot without interpolation in the lower panel. (b) Optical conductivity spectra of TM_2AsF_6 , TM_2PF_6 , and TM_2SbF_6 . Triangles and shaded regions indicate the SR peaks and their Lorentzian fits, respectively. Spectra at higher temperatures are vertically offset for clarity (dashed lines indicate their zeros). (c) Temperature dependences. Top panel: Time-domain waveforms of THz electric field E_{THz} emitted from TM_2AsF_6 . Lower panels: Spectral intensities of E_{THz} and SR peak intensities, for TM_2AsF_6 , TM_2PF_6 , and TM_2SbF_6 .

intermolecular translations, respectively. Among them, the SR peak is the most useful probe of CO for its largest change against temperature. Similarly, for the analogous compound TM_2PF_6 , peaks were observed in the vicinity at $22\text{ K} \ll T_{\text{CO}}$; the 70-cm^{-1} peak should be assigned to the T_c mode or the SR peak, for its largest increase across T_{CO} as the SR peak of TM_2AsF_6 . Given that the peak redshifts with increasing anion size, a lower frequency is expected for TM_2SbF_6 with the larger size. Accordingly, the intensity of the 64-cm^{-1} peak ($20\text{ K} \ll T_{\text{CO}}$) shows the largest increase against temperature, hence it is reasonably assigned to the SR peak. The systematic shift is explicitly shown in Fig. S1 [43].

It is reasonable that the SR peak does not soften around T_{CO} . In a displacive-type ferroelectrics, a soft mode is an *optical* phonon whose motion modulates potential P . In contrast, the intermolecular vibration causing the SR peak is *not* infrared active until the charge disproportionation sets in around T_{CO} ; hence it cannot be a soft mode, despite its sensitivity to P .

It should be noted that the SR peaks are evident even slightly above T_{CO} (130 K for TM_2AsF_6 and 80 K for TM_2PF_6); the continuous change from $T \ll T_{\text{CO}}$ is confirmed by absorption spectra measured in 1-K steps [Fig. 2(a)]. This is consistent with the fact that short-range correlations in general start to develop above the phase transition temperature in low dimensions [44]; intradimer charge disproportionation would randomly take place above T_{CO} , and the fluctuations slower than the peak frequency ($\sim 1/\text{ps}$) bear their infrared activity. Such a temperature evolution of the short-range correlations is also clearly seen in the lower three panels of Fig. 2(c), where we plot the peak intensities estimated by a Lorentzian fit [shaded regions in Fig. 2(b)] to exclude contributions of adjacent peaks and background.

Although the preceding study on a one-dimensional system has pointed out a divergent increase of infrared activity near the transition [45], we could not identify it in the observed spectra [46].

Unlike diffraction experiments [47,48], the SR peak alone can hardly disentangle contributions from the short- and long-range correlations. To resolve this, we also measured the THz emission triggered by femtosecond pulses [Fig. 1(b)]. The color map shown in the top panel of Fig. 2(c) represents the time-domain waveforms of the THz electric field $E_{\text{THz}}(t)$ emitted from TM_2AsF_6 . E_{THz} became nonzero below T_{CO} , where CO accompanies macroscopic P breaking spatial inversion symmetry. Hence the emission process is attributable to optical rectification via second-order nonlinear susceptibility $\chi^{(2)}(\omega - \omega)$, which in general becomes nonzero upon losing centrosymmetry [49–51]. Accordingly the emission intensity showed the expected quadratic increase with incident light fluence, as shown in Fig. S2 [43].

Note that the E_{THz} signal arises from the CO with long-range space correlations; a THz wave from a bunch of nanoscaled domains having antiparallel P (antiphase charge configuration) will destructively interfere and cancel out, since inversion of P will invert the sign of $\chi^{(2)}$ or the resultant E_{THz} . This behavior is distinct from the SR peak absorption, which is activated by intradimer charge disproportionation irrespective of its phase.

To confirm the long-range correlations, we performed THz-emission microscopy. By focusing the fundamental

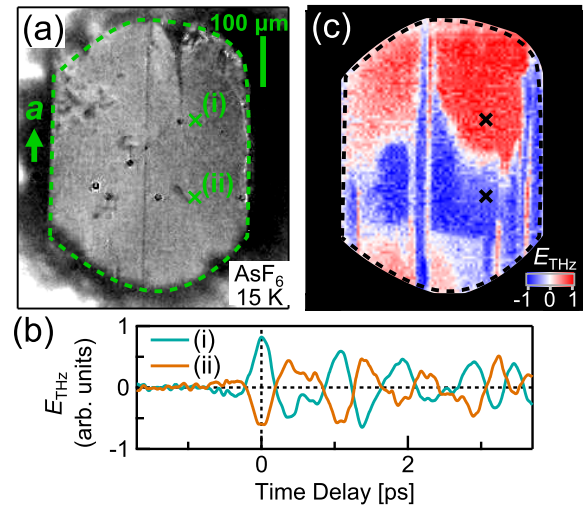


FIG. 3. (a) Reflection image of TM_2AsF_6 sample at 15 K. (b) Time-domain THz waveforms observed by irradiating the positions (i) and (ii) with fundamental light having a $5\text{-}\mu\text{m}$ -diameter spot focused by an objective lens (numerical aperture $\text{NA} = 0.13$). The fluence was 5 mJ/cm^2 . (c) Raster scan of THz emission: $5\text{-}\mu\text{m}$ -step map of $E_{\text{THz}}(0\text{ ps})$.

beam onto TM_2AsF_6 , THz emission occurs from the irradiated $5\text{-}\mu\text{m}$ spot, e.g. position (i) or (ii) shown in Fig. 3(a). As shown in Fig. 3(b), the resultant E_{THz} exhibited a position-dependent sign reversal. This should be due to the inversion of $\chi^{(2)}$ upon inversion of the order parameter P ; hence the $E_{\text{THz}}(0\text{ ps})$ value works as a measure of the sign of P [52]. As shown in Fig. 3(c), its color map, or raster scan of the THz emission, clearly evidences antiparallel P domains with correlations as long as hundreds of microns in the ab plane. Such large domains can avoid the cancellation effect, and in fact, the E_{THz} signal was successfully observed even in nonmicroscopy measurements [Fig. 2(c)] reflecting the long-range CO (see Supplemental Material for a quantitative characterization [43]).

In the lower three panels of Fig. 2(c), we plot the intensities of the amplitude spectra $E_{\text{THz}}(\omega)$, the Fourier transform of time-domain waveforms, for all compounds (see Figs. S2–S4 for spectral shapes). The onsets of E_{THz} are almost at T_{CO} , in contrast to those of the SR peak intensity which are $\sim 50\text{ K}$ above T_{CO} . This unambiguously demonstrates that the short-range correlations develop above T_{CO} activating the SR peak, followed by the formation of the long-range CO triggering THz emission below T_{CO} . Therefore they provide complementary insight on the charge dynamics.

The development of CO has been quantitatively studied by midinfrared and Raman spectroscopy via *intramolecular* phonon modes showing a charge-sensitive frequency shift or consequent splitting [32,53–58]. Therein no particular attention was paid to the behavior above T_{CO} , probably because it is not easy to identify a weak satellite peak with a small shift compared to its width. In contrast, the SR peak, which is *intermolecular* vibration focused in this work, is not hindered by such an overlap and hence the development of its intensity could sensitively be captured [59].

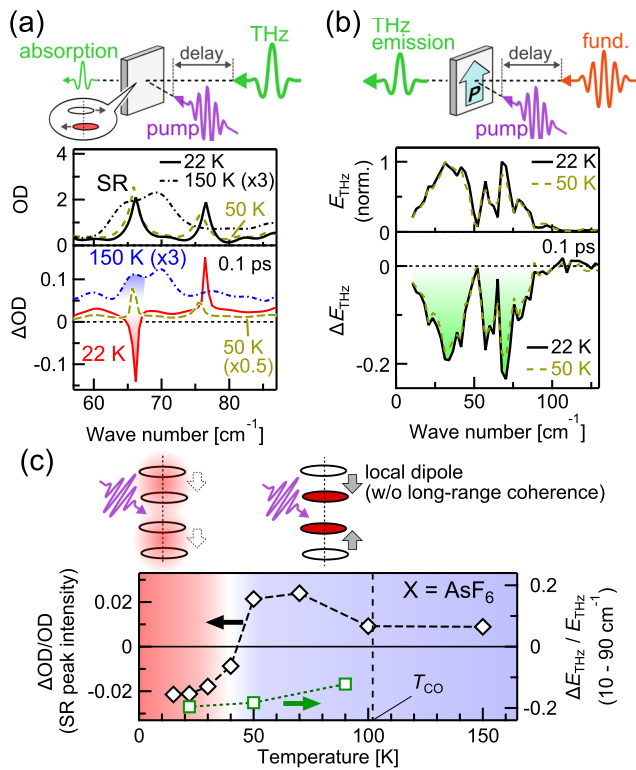


FIG. 4. (a) and (b) show the schematics of the optical-pump THz-absorption-probe and THz-emission-probe experiment, respectively, and the results for TM_2AsF_6 . The upper and lower panel show steady-state THz absorption (emission) spectra and their photoinduced change, respectively. OD at 150 K is vertically offset by -2.6 for clarity. (c) Temperature dependence of the photoinduced changes of the SR peak intensity (left axis) and THz emission (right axis). The schematics show the photoinduced charge dynamics therein.

Having identified the probes for short- and long-range charge correlations, we can now study their photoinduced dynamics. To that end we measured the photoinduced change of THz absorption and emission as schematically shown in Figs. 4(a) and 4(b), respectively, without the contribution of the pump-pulse-induced THz emission [60]. The 0.89-eV pump light ($|a$) above the CO gap $\Delta_{\text{CO}} \sim 0.1$ eV [31] corresponds to the charge transfer excitation [61]. The pump fluence was 0.2 mJ/cm^2 ; the laser heating effect does not affect the following discussions, wherein the resultant rise of crystal temperature is as small as ~ 5 K [43]. It is known that the temporal resolution of transient THz time-domain measurements can be as good as the pump duration, currently 0.1 ps, despite a chirped THz probe pulse with a duration of several picoseconds [62,63] (see Supplemental Material for details [43]).

Figure 4(a) shows steady-state absorption spectra of TM_2AsF_6 around the SR peak (upper panel), and their changes at 0.1 ps (pump pulse duration) after photoexcitation (lower panel). At 22 K well below T_{CO} , the SR peak was suppressed upon photoexcitation (red line). Since such suppression was absent in the adjacent phonon peak at $\sim 76 \text{ cm}^{-1}$, the result cannot be accounted for by laser heating or by screening due to photocarriers which presumably

caused broad photoabsorption of $\Delta\text{OD} \sim 0.02$. Therefore the suppression should be due to a photoinduced dissolution of intradimer charge disproportionation hosting the infrared activity of the SR peak. In striking contrast, at $150 \text{ K} > T_{\text{CO}}$ where charges only have short-range correlations without long-range CO, the SR peak was enhanced within 0.1 ps after photoexcitation (blue dashed-dotted line). Since the change is contrary to the suppression, it is reasonable to assign the result to a photoinduced enhancement of the short-range correlations. The electronic response should be dominant in these instantaneous changes, since the timescale is much shorter than a period of the SR mode, $(\sim 70 \text{ cm}^{-1})^{-1} \sim 0.5$ ps, which is the minimum duration required to define the peak frequency. Time evolutions of ΔOD are shown in Fig. S6 [43].

Since the peak at higher frequency ($\sim 76 \text{ cm}^{-1}$ at 22 K) has not yet been assigned, its photoinduced change remains unresolved at present; however, it is likely insensitive to the photoinduced charge dynamics, since it does not show a noticeable change around T_{CO} in the steady-state spectra [Fig. 2(a)].

Figure 4(b) shows, in the same manner as Fig. 4(a), the E_{THz} spectra and their changes at 0.1 ps after photoexcitation. At $T = 22$ K, E_{THz} was suppressed over the whole spectral range, indicating that macroscopic \mathbf{P} vanishes upon photoexcitation; the result is consistent with the dissolution of short-range correlations [Fig. 4(a)] which inevitably collapses long-range CO. Although such a collapse is known to accompany a photoinduced insulator-metal transition in another system [50,64,65], we currently cannot judge whether or not the photoinduced state is metallic before observing the THz dynamics along the conducting a axis.

Figure 4(c) summarizes the temperature dependences. With T increasing from 15 K, the photoinduced change of the SR peak turns from suppression to enhancement near 40 K below T_{CO} , and the enhancement is also observed around and above T_{CO} . This reveals that the photoinduced change of the short-range CO undergoes a crossover; the crossing temperature ~ 40 K reflecting the competition between the suppression and enhancement is characteristic of the photoinduced states, and accordingly equilibrium data show no anomaly around the temperature (Fig. 2). Although CO in the higher-temperature side is closer to its thermal melting point at T_{CO} , the short-range fluctuations therein are actually enhanced upon photoexcitation. Its amount tends to become smaller at higher temperature; to resolve the detail, a further study including sample dependence is required. On the other hand, THz emission or long-range CO was suppressed irrespective of temperature. Note that the signs of ΔOD and ΔE_{THz} are opposite above 40 K, for example, at 50 K as seen in Figs. 4(a) and 4(b) (yellow dashed lines). This is explained by the difference in spatial scale; upon photoexcitation the charge distribution was randomized to have a larger intradimer disproportionation than before, while long-range ($\sim \mu\text{m}$) coherence was lost, canceling macroscopic \mathbf{P} .

The amount of photoinduced change is closely related to the volume fraction of the photoexcited surface. It is estimated as $\sim 0.4\%$ for a typical sample thickness of $100 \mu\text{m}$, using a penetration depth $d \sim 0.4 \mu\text{m}$ at 0.89 eV calculated from the result of a Kramers-Kronig analysis [66]. Hence the $\sim 2\%$ decrease of the SR peak intensity [Fig. 4(c)] suggests that

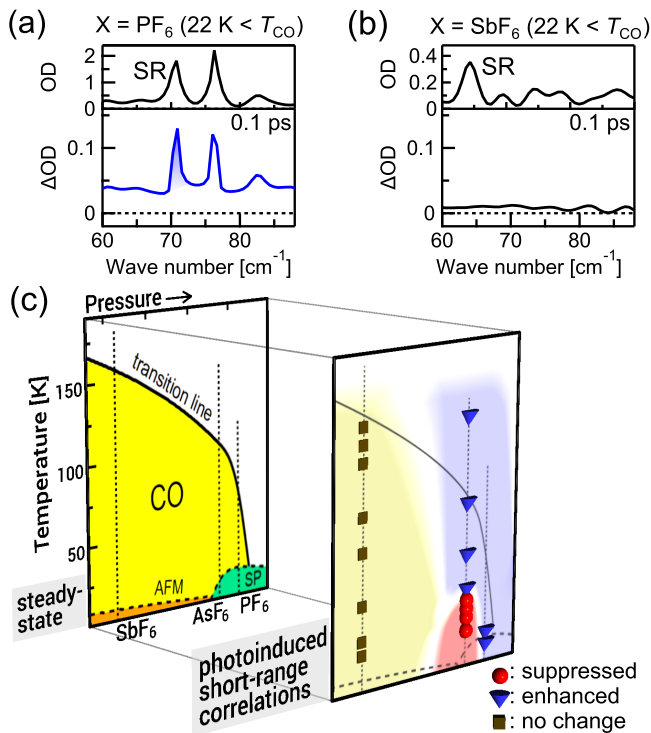


FIG. 5. (a) and (b) show results of the optical-pump THz-absorption-probe experiments for TM_2PF_6 and TM_2SbF_6 , respectively, shown in the same way as Fig. 4(a). (c) Left: Steady-state temperature-pressure phase diagram of TM_2X (reproduced from Ref. [32]). AFM: antiferromagnet; SP: Spin Peierls. Right: Photoinduced change of the SR peak superimposed on the diagram. Red spheres: suppressed; blue cones: Enhanced; brown boxes: no change.

CO was almost completely dissolved. Therein the photon number was estimated as small as ~ 0.005 per TM molecule, implying that cooperative phenomena took place as in other photoinduced phase transition processes [17], although a fluence-dependent study is required for a detailed discussion. For THz emission, the volume fraction of the photoinduced area is effectively $\sim 100\%$ because d for 1.55-eV fundamental light is comparable to that for the pump light [66], hence a larger photoinduced change is expected, as observed ($\sim 20\%$). A quantitative comparison of the photoinduced changes requires an analysis of domain structures, which is beyond the scope of this Letter.

To gain deeper insight into the characteristic enhancement of the short-range correlations, we performed the same experiments on other compounds. As shown in Fig. 5(a), the SR peak of TM_2PF_6 at 22 K was enhanced within 0.1 ps after photoexcitation; on changing the anion from AsF_6 to PF_6 , i.e.,

applying chemical pressure, the peak suppression [Fig. 4(a)] turns into the enhancement. This inversion resembles that observed for TM_2AsF_6 during heating [Fig. 4(c)], both of which correspond to approaching the CO transition line in the phase diagram [left panel of Fig. 5(c), reproduced from Ref. [32]]. The magnetic contribution should be absent in the inversion, since the result was invariant at a lower temperature below the spin-Peierls transition (Fig. S7 [43]). For TM_2SbF_6 located in the lower-pressure region, no change was identified in the SR peak [Figs. 5(b) and 5(c)]. THz emission of these compounds, on the other hand, was suppressed as in TM_2AsF_6 (Fig. S6 [43]), indicating that long-range CO is always collapsed upon photoexcitation irrespective of chemical pressure or temperature. The collapse without the SR peak suppression is attributable to the randomization of the short-range correlations [Fig. 4(c)], although the correlations in TM_2SbF_6 do not appear to be enhanced. The photoinduced change had a timescale of several picoseconds and was insensitive to temperature nor anion (Fig. S6 [43]).

In Fig. 5(c) we show on the left-hand side the steady-state temperature-pressure phase diagram reproduced from Ref. [32], while on the right-hand side we superimposed the results of the photoinduced changes of the SR peak on the diagram (original data are shown in Fig. S7 [43]). The suppression was observed only for TM_2AsF_6 at low temperatures in the CO phase (red spheres), where intradimer charge disproportionation is dissolved. With increasing temperature or pressure toward the CO phase boundary, it turned into the enhancement (blue cones). Meanwhile, when the pressure is small, no change was identified even near T_{CO} (brown boxes).

The various photoresponses of the short-range CO were found to be sensitive not only to temperature but also to pressure or the resultant electronic parameters, showing the distinctive distribution from the steady-state phase diagram. This opens up an extra route toward tailoring unprecedented nonequilibrium states, which is based on another idea rather than the suppression of competing phases as seen in the photoinduced superconductivity [67]. Although recent theoretical studies have succeeded in showing that the photoinduced modulation of short-range charge correlations is feasible [61,68,69], further investigations are indispensable to quantitatively understand the observed crossover against temperature and chemical pressure.

This work was supported by Japan Science and Technology agency (JST) CREST (JPMJCR1901), MEXT Q-LEAP (JPMXS0118067426), Japan Society for the Promotion of Science (JSPS) KAKENHI (Grants No. JP15H02100, No. JP17K14317, No. JP18H01144, No. JP20K03800, and No. JP20H05147), Hattori Hokokai Foundation, and Toyota Riken Scholar. The work at Universität Stuttgart was supported by the DFG via DR228/39-3.

- [1] E. Dagotto, Complexity in strongly correlated electronic systems, *Science* **309**, 257 (2005).
 [2] M. Liu, A. J. Sternbach, and D. N. Basov, Nanoscale electro-dynamics of strongly correlated quantum materials, *Rep. Prog. Phys.* **80**, 014501 (2017).

- [3] A. S. McLeod, E. van Heumen, J. G. Ramirez, S. Wang, T. Saerbeck, S. Guenon, M. Goldflam, L. Andereg, P. Kelly, A. Mueller, M. K. Liu, I. K. Schuller, and D. N. Basov, Nanotextured phase coexistence in the correlated insulator V_2O_3 , *Nat. Phys.* **13**, 80 (2017).

- [4] A. Pustogow, A. S. McLeod, Y. Saito, D. N. Basov, and M. Dressel, Internal strain tunes electronic correlations on the nanoscale, *Sci. Adv.* **4**, eaau9123 (2018).
- [5] B. Keimer, S. A. Kivelson, M. R. Norman, S. Uchida, and J. Zaanen, From quantum matter to high-temperature superconductivity in copper oxides, *Nature (London)* **518**, 179 (2015).
- [6] Y. Tokura, Critical features of colossal magnetoresistive manganites, *Rep. Prog. Phys.* **69**, 797 (2006).
- [7] R. A. Cowley, S. N. Gvasaliya, S. G. Lushnikov, B. Roessli, and G. M. Rotaru, Relaxing with relaxors: a review of relaxor ferroelectrics, *Adv. Phys.* **60**, 229 (2011).
- [8] M. Dressel and A. Pustogow, Electrodynamics of quantum spin liquids, *J. Phys.: Condens. Matter* **30**, 203001 (2018).
- [9] N. Hassan, S. Cunningham, M. Mourigal, E. I. Zhilyaeva, S. A. Torunova, R. N. Lyubovskaya, J. A. Schlueter, and N. Drichko, Evidence for a quantum dipole liquid state in an organic quasi-two-dimensional material, *Science* **360**, 1101 (2018).
- [10] F. Kagawa, T. Sato, K. Miyagawa, K. Kanoda, Y. Tokura, K. Kobayashi, R. Kumai, and Y. Murakami, Charge-cluster glass in an organic conductor, *Nat. Phys.* **9**, 419 (2013).
- [11] S. Sasaki, K. Hashimoto, R. Kobayashi, K. Itoh, S. Iguchi, Y. Nishio, Y. Ikemoto, T. Moriwaki, N. Yoneyama, M. Watanabe, A. Ueda, H. Mori, K. Kobayashi, R. Kumai, Y. Murakami, J. Müller, and T. Sasaki, Crystallization and vitrification of electrons in a glass-forming charge liquid, *Science* **357**, 1381 (2017).
- [12] K. Nasu, Itinerant type many-body theories for photo-induced structural phase transitions, *Rep. Prog. Phys.* **67**, 1607 (2004).
- [13] M. Kuwata-Gonokami and S. Koshihara (eds.), Special issue on photo-induced phase transitions and their dynamics, *J. Phys. Soc. Jpn.* **75**, issue 1 (2006).
- [14] C. Giannetti, M. Capone, D. Fausti, M. Fabrizio, F. Parmigiani, and D. Mihailovic, Ultrafast optical spectroscopy of strongly correlated materials and high-temperature superconductors: A non-equilibrium approach, *Adv. Phys.* **65**, 58 (2016).
- [15] M. C. Langner, S. Zhou, G. Coslovich, Y.-D. Chuang, Y. Zhu, J. S. Robinson, W. F. Schlotter, J. J. Turner, M. P. Minitti, R. G. Moore, W. S. Lee, D. H. Lu, D. Doering, P. Denes, Y. Tomioka, Y. Tokura, R. A. Kaindl, and R. W. Schoenlein, Ultrafast x-ray and optical signatures of phase competition and separation underlying the photoinduced metallic phase in $\text{Pr}_{1-x}\text{Ca}_x\text{MnO}_3$, *Phys. Rev. B* **92**, 155148 (2015).
- [16] S. D. Conte, L. Vidmar, D. Golež, M. Mierzejewski, G. Soavi, S. Peli, F. Banfi, G. Ferrini, R. Comin, B. M. Ludbrook, L. Chauviere, N. D. Zhigadlo, H. Eisaki, M. Greven, S. Lupi, A. Damascelli, D. Brida, M. Capone, J. Bonča, G. Cerullo *et al.*, Snapshots of the retarded interaction of charge carriers with ultrafast fluctuations in cuprates, *Nat. Phys.* **11**, 421 (2015).
- [17] S. Iwai, K. Yamamoto, A. Kashiwazaki, F. Hiramatsu, H. Nakaya, Y. Kawakami, K. Yakushi, H. Okamoto, H. Mori, and Y. Nishio, Photoinduced Melting of a Stripe-Type Charge-Order and Metallic Domain Formation in a Layered BEDT-TTF-Based Organic Salt, *Phys. Rev. Lett.* **98**, 097402 (2007).
- [18] H. Nakaya, K. Itoh, Y. Takahashi, H. Itoh, S. Iwai, S. Saito, K. Yamamoto, and K. Yakushi, Terahertz responses of the high-temperature metallic phase and photoinduced metallic state in the ferroelectric charge-ordered organic salt α -(ET) $_2$ I $_3$, *Phys. Rev. B* **81**, 155111 (2010).
- [19] Y. Kawakami, T. Fukatsu, Y. Sakurai, H. Unno, H. Itoh, S. Iwai, T. Sasaki, K. Yamamoto, K. Yakushi, and K. Yonemitsu, Early-Stage Dynamics of Light-Matter Interaction Leading to the Insulator-to-Metal Transition in a Charge Ordered Organic Crystal, *Phys. Rev. Lett.* **105**, 246402 (2010).
- [20] Y. Wang, C.-C. Chen, B. Moritz, and T. P. Devereaux, Light-Enhanced Spin Fluctuations and d-Wave Superconductivity at a Phase Boundary, *Phys. Rev. Lett.* **120**, 246402 (2018).
- [21] T. Ishikawa, Y. Sagae, Y. Naitoh, Y. Kawakami, H. Itoh, K. Yamamoto, K. Yakushi, H. Kishida, T. Sasaki, S. Ishihara, Y. Tanaka, K. Yonemitsu, and S. Iwai, Optical freezing of charge motion in an organic conductor, *Nat. Commun.* **5**, 5528 (2014).
- [22] Y. Naitoh, Y. Kawakami, T. Ishikawa, Y. Sagae, H. Itoh, K. Yamamoto, T. Sasaki, M. Dressel, S. Ishihara, Y. Tanaka, K. Yonemitsu, and S. Iwai, Ultrafast response of plasmalike reflectivity edge in $(\text{TMTTF})_2\text{AsF}_6$ driven by a 7-fs 1.5-cycle strong-light field, *Phys. Rev. B* **93**, 165126 (2016).
- [23] H. Ichikawa, S. Nozawa, T. Sato, A. Tomita, K. Ichiyangi, M. Chollet, L. Guerin, N. Dean, A. Cavalleri, S. Adachi, T. Arima, H. Sawa, Y. Ogimoto, M. Nakamura, R. Tamaki, K. Miyano, and S. Koshihara, Transient photoinduced “hidden” phase in a manganite, *Nat. Mater.* **10**, 101 (2011).
- [24] T.-R. T. Han, F. Zhou, C. D. Malliakas, P. M. Duxbury, S. D. Mahanti, M. G. Kanatzidis, and C.-Y. Ruan, Exploration of metastability and hidden phases in correlated electron crystals visualized by femtosecond optical doping and electron crystallography, *Sci. Adv.* **1**, e1400173 (2015).
- [25] D. Fausti, R. I. Tobey, N. Dean, S. Kaiser, A. Dienst, M. C. Hoffmann, S. Pyon, T. Takayama, H. Takagi, and A. Cavalleri, Light-induced superconductivity in a stripe-ordered cuprate, *Science* **331**, 189 (2011).
- [26] Z. Sun and A. J. Millis, Transient Trapping into Metastable States in Systems with Competing Orders, *Phys. Rev. X* **10**, 021028 (2020).
- [27] S. A. Dönges, O. Khatib, B. T. O’Callahan, J. M. Atkin, J. H. Park, D. Cobden, and M. B. Raschke, Ultrafast nanoimaging of the photoinduced phase transition dynamics in VO_2 , *Nano Lett.* **16**, 3029 (2016).
- [28] A. Zong, A. Kogar, Y.-Q. Bie, T. Rohwer, C. Lee, E. Baldini, E. Ergeçen, M. B. Yilmaz, B. Freelon, E. J. Sie, H. Zhou, J. Straquadine, P. Walmsley, P. E. Dolgirev, A. V. Rozhkov, I. R. Fisher, P. Jarillo-Herrero, B. V. Fine, and N. Gedik, Evidence for topological defects in a photoinduced phase transition, *Nat. Phys.* **15**, 27 (2019).
- [29] Y. A. Gerasimenko, P. Karpov, I. Vaskivskiy, S. Brazovskii, and D. Mihailovic, Intertwined chiral charge orders and topological stabilization of the light-induced state of a prototypical transition metal dichalcogenide, *npj Quantum Mater.* **4**, 32 (2019).
- [30] T. Ishikawa, S. A. Hayes, S. Keskin, G. Corthey, M. Hada, K. Pichugin, A. Marx, J. Hirscht, K. Shionuma, K. Onda, Y. Okimoto, S. Koshihara, T. Yamamoto, H. Cui, M. Nomura, Y. Oshima, M. Abdel-Jawad, R. Kato, and R. J. D. Miller, Direct observation of collective modes coupled to molecular orbital-driven charge transfer, *Science* **350**, 1501 (2015).
- [31] B. Köhler, E. Rose, M. Dumm, G. Untereiner, and M. Dressel, Comprehensive transport study of anisotropy and ordering phenomena in quasi-one-dimensional $(\text{TMTTF})_2\text{X}$ salts ($X = \text{PF}_6, \text{AsF}_6, \text{SbF}_6, \text{BF}_4, \text{ClO}_4, \text{ReO}_4$), *Phys. Rev. B* **84**, 035124 (2011).
- [32] M. Dressel, M. Dumm, T. Knoblauch, and M. Masino, Comprehensive optical investigations of charge order in organic chain compounds $(\text{TMTTF})_2\text{X}$, *Crystals* **2**, 528 (2012).

- [33] P. Monceau, F. Y. Nad, and S. Brazovskii, Ferroelectric Mott-Hubbard Phase of Organic (TMTTF)₂X Conductors, *Phys. Rev. Lett.* **86**, 4080 (2001).
- [34] H. Seo, C. Hotta, and H. Fukuyama, Toward systematic understanding of diversity of electronic properties in low-dimensional molecular solids, *Chem. Rev.* **104**, 5005 (2004).
- [35] S. Ishihara, Electronic ferroelectricity in molecular organic crystals, *J. Phys.: Condens. Matter* **26**, 493201 (2014).
- [36] S. Tomić and M. Dressel, Ferroelectricity in molecular solids: A review of electrodynamic properties, *Rep. Prog. Phys.* **78**, 096501 (2015).
- [37] R. Rösslhuber, E. Rose, T. Ivek, A. Pustogow, T. Breier, M. Geiger, K. Schrem, G. Untereiner, and M. Dressel, Structural and electronic properties of (TMTTF)₂X salts with tetrahedral anions, *Crystals* **8**, 121 (2018).
- [38] R. Laversanne, C. Coulon, B. Gallois, J. P. Pouget, and R. Moret, Structural and electrical properties of (TMTTF)₂MF₆ salts (M = P, As, Sb). Role of the anions, *J. Phys. Lett.* **45**, 393 (1984).
- [39] B. Liautard, S. Peytavin, G. Brun, and M. Maurin, Tetramethyl-tetrathiofulvalene hexafluoroarsenate, (C₁₀H₁₂S₄)₂AsF₆, *Cryst. Struct. Commun.* **11**, 1841 (1982).
- [40] B. Liautard, S. Peytavin, G. Brun, and M. Maurin, Corrélations structurales dans la série (TMTTF)₂X, *J. Phys. IV France* **43**, 1453 (1982).
- [41] S. Kitou, T. Fujii, T. Kawamoto, N. Katayama, S. Maki, E. Nishibori, K. Sugimoto, M. Takata, T. Nakamura, and H. Sawa, Successive Dimensional Transition in (TMTTF)₂PF₆ Revealed by Synchrotron X-ray Diffraction, *Phys. Rev. Lett.* **119**, 065701 (2017).
- [42] T. Granier, B. Gallois, L. Ducasse, A. Fritsch, and A. Filhol, 4 K crystallographic and electronic structures of (TMTTF)₂X salts (X⁻: PF₆⁻, AsF₆⁻), *Synth. Met.* **24**, 343 (1988).
- [43] See Supplemental Material at <http://link.aps.org/supplemental/10.1103/PhysRevResearch.3.L032043> for (1) the experimental details, (2) the systematic shift of the SR peak, (3) the detailed characteristics of the THz emission, (4) discussions on the length scale of the long-range charge correlations, (5) the estimation of the laser heating, (6) the time evolutions of the photoinduced changes, (7) the photoinduced spectra used in Fig. 5(c), and (8) a discussion on the temperature dependence below T_{CO}.
- [44] G. Coslovich, B. Huber, W.-S. Lee, Y. -D. Chuang, Y. Zhu, T. Sasagawa, Z. Hussain, H. A. Bechtel, M. C. Martin, Z. -X. Shen, R. W. Schoenlein, and R. A. Kaindl, Ultrafast charge localization in a stripe-phase nickelate, *Nat. Commun.* **4**, 2643 (2013).
- [45] L. DeIreo, A. Painelli, and Z. G. Soos, Giant Infrared Intensity of the Peierls Mode at the Neutral-Ionic Phase Transition, *Phys. Rev. Lett.* **89**, 027402 (2002).
- [46] It has been theoretically pointed out that, in the mixed-stack system, the infrared intensity of the dimerization mode divergently increases near the transition point [45]. The absence of such behavior near T_{CO} (Fig. 2) could be due to the difference in the lattice structure; TM₂X consists of single-component molecular chains with TM dimers, unlike the aforementioned donor-acceptor stack. The observation also suggests that CO-to-non-CO domain wall excitations, which may be enhanced near T_{CO}, were out of the current THz range, if any. Although a charged soliton separating antiphase CO domains may also emerge below T_{CO} [36], we speculate that it is difficult to identify; since the CO domains are comparably large to the crystal size [Fig. 3(c)], the solitons might have a small volume fraction, and concomitantly have weak infrared activity to be masked by the intermolecular vibrations.
- [47] S. Wall, S. Yang, L. Vidas, M. Chollet, J. M. Glowia, M. Kozina, T. Katayama, T. Henighan, M. Jiang, T. A. Miller, D. A. Reis, L. A. Boatner, O. Delaire, and M. Trigo, Ultrafast disordering of vanadium dimers in photoexcited VO₂, *Science* **362**, 572 (2018).
- [48] L. Guérin, J. Hébert, M. Buron-LeCointe, S. I. Adachi, S. Y. Koshihara, H. Cailleau, and E. Collet, Capturing One-Dimensional Precursors of a Photoinduced Transformation in a Material, *Phys. Rev. Lett.* **105**, 246101 (2010).
- [49] R. W. Boyd, *Nonlinear Optics*, 3rd ed. (Academic, New York, 2008).
- [50] H. Itoh, K. Itoh, K. Goto, K. Yamamoto, K. Yakushi, and S. Iwai, Efficient terahertz-wave generation and its ultrafast optical modulation in charge ordered organic ferroelectrics, *Appl. Phys. Lett.* **104**, 173302 (2014).
- [51] In a triclinic crystal all of the χ⁽²⁾ tensor components are nonzero [49]. Hence the THz emission along the b' axis may occur as observed, although it is perpendicular to the molecular stacks (the a axis) or the expected direction of macroscopic polarization P.
- [52] M. Sotome, N. Kida, S. Horiuchi, and H. Okamoto, Visualization of ferroelectric domains in a hydrogen-bonded molecular crystal using emission of terahertz radiation, *Appl. Phys. Lett.* **105**, 041101 (2014).
- [53] M. Meneghetti, R. Bozio, I. Zanon, C. Pecile, C. Ricotta, and M. Zanetti, Vibrational behavior of molecular constituents of organic superconductors: TMTSF, its radical cation and the sulphur analogs TMTTF and TMTTF⁺, *J. Chem. Phys.* **80**, 6210 (1984).
- [54] S. Hirose, A. Kawamoto, N. Matsunaga, K. Nomura, K. Yamamoto, and K. Yakushi, Reexamination of ¹³C-NMR in (TMTTF)₂AsF₆: Comparison with infrared spectroscopy, *Phys. Rev. B* **81**, 205107 (2010).
- [55] M. Dumm, M. Abaker, M. Dressel, and L. K. Montgomery, Charge order in (TMTTF)₂PF₆ investigated by infrared spectroscopy, *J. Low Temp. Phys.* **142**, 609 (2006).
- [56] T. Knoblauch and M. Dressel, Charge disproportionation in (TMTTF)₂X (X = PF₆, AsF₆ and SbF₆) investigated by infrared spectroscopy, *Phys. Status Solidi C* **9**, 1158 (2012).
- [57] M. Dumm, B. Salameh, M. Abaker, L. K. Montgomery, and M. Dressel, Magnetic and optical studies of spin and charge ordering in (TMTTF)₂AsF₆, *J. Phys. IV France* **114**, 57 (2004).
- [58] R. Świątlik, B. Barszcz, A. Pustogow, and M. Dressel, Raman spectroscopy evidence of domain walls in the organic electronic ferroelectrics (TMTTF)₂X (X = SbF₆, AsF₆, PF₆), *Phys. Rev. B* **95**, 085205 (2017).
- [59] While charge disproportionation above T_{CO} has not been reported in NMR studies [70–72], the electron spin resonance (ESR) study has succeeded in observing a corresponding signal [73]. One reason may be a slow timescale of NMR measurements (typically in the MHz range) compared to the current THz measurements or ESR measurements (~10 GHz), which might hinder dynamic charge fluctuations faster than a nanosecond timescale.

- [60] The THz detector senses a linear superposition of the probe THz light and the pump-beam-induced THz emission. In order to filter out the latter contribution from the signal, an incident probe beam was modulated with an optical chopper in both experiments.
- [61] T. Yamaguchi, K. Asada, H. Yamakawa, T. Miyamoto, K. Iwano, T. Nakamura, N. Kida, and H. Okamoto, Photoexcitation of a one-dimensional polarization-inverted domain from the charge-ordered ferroelectric ground state of $(\text{TMTTF})_2\text{PF}_6$, *Phys. Rev. B* **99**, 245104 (2019).
- [62] J. T. Kindt and C. A. Schmuttenmaer, Theory for determination of the low-frequency time-dependent response function in liquids using time-resolved terahertz pulse spectroscopy, *J. Chem. Phys.* **110**, 8589 (1999).
- [63] G. Coslovich, A. F. Kemper, S. Behl, B. Huber, H. A. Bechtel, T. Sasagawa, M. C. Martin, A. Lanzara, and R. A. Kaindl, Ultrafast dynamics of vibrational symmetry breaking in a charge-ordered nickelate, *Sci. Adv.* **3**, e1600735 (2017).
- [64] K. Yamamoto, S. Iwai, S. Boyko, A. Kashiwazaki, F. Hiramatsu, C. Okabe, N. Nishi, and K. Yakushi, Strong optical nonlinearity and its ultrafast response associated with electron ferroelectricity in an organic conductor, *J. Phys. Soc. Jpn.* **77**, 074709 (2008).
- [65] H. Itoh, R. Fujiwara, Y. Kawakami, K. Yamamoto, Y. Nakamura, H. Kishida, and S. Iwai, Modulation of terahertz emission in time-domain waveform via a photoinduced phase transition in a charge ordered organic ferroelectric, *Appl. Phys. Lett.* **112**, 093302 (2018).
- [66] V. Vescoli, L. Degiorgi, K. P. Starkey, and L. K. Montgomery, Anisotropy in the optical response of $(\text{TMTTF})_2\text{X}$ ($\text{X} = \text{PF}_6$ and Br) Bechgaard salts, *Solid State Commun.* **111**, 507 (1999).
- [67] M. Först, R. I. Tobey, H. Bromberger, S. B. Wilkins, V. Khanna, A. D. Caviglia, Y.-D. Chuang, W. S. Lee, W. F. Schlotter, J. J. Turner, M. P. Minitti, O. Krupin, Z. J. Xu, J. S. Wen, G. D. Gu, S. S. Dhesi, A. Cavalleri, and J. P. Hill, Melting of Charge Stripes in Vibrationally Driven $\text{La}_{1.875}\text{Ba}_{0.125}\text{CuO}_4$: Assessing the Respective Roles of Electronic and Lattice Order in Frustrated Superconductors, *Phys. Rev. Lett.* **112**, 157002 (2014).
- [68] C. Shao, H. Lu, H.-G. Luo, and R. Mondaini, Photoinduced enhancement of bond order in the one-dimensional extended Hubbard model, *Phys. Rev. B* **100**, 041114(R) (2019).
- [69] M. Schüler, Y. Murakami, and P. Werner, Nonthermal switching of charge order: Dynamical slowing down and optimal control, *Phys. Rev. B* **97**, 155136 (2018).
- [70] D. S. Chow, F. Zamborszky, B. Alavi, D. J. Tantillo, A. Baur, C. A. Merlic, and S. E. Brown, Charge Ordering in the TMTTF Family of Molecular Conductors, *Phys. Rev. Lett.* **85**, 1698 (2000).
- [71] F. Zamborszky, W. Yu, W. Raas, S. E. Brown, B. Alavi, C. A. Merlic, A. Baur, S. Lefebvre, and P. Wzietek, Influence of charge order on the ground state of TMTTF conductors, *J. Phys. IV France* **12**, 139 (2002).
- [72] S. Fujiyama and T. Nakamura, Redistribution of electronic charges in spin-Peierls state in $(\text{TMTTF})_2\text{AsF}_6$ observed by ^{13}C NMR, *J. Phys. Soc. Jpn.* **75**, 014705 (2006).
- [73] S. Yasin, B. Salameh, E. Rose, M. Dumm, H.-A. Krug von Nidda, A. Loidl, M. Ozerov, G. Untereiner, L. Montgomery, and M. Dressel, Broken magnetic symmetry due to charge-order ferroelectricity discovered in $(\text{TMTTF})_2\text{X}$ salts by multifrequency ESR, *Phys. Rev. B* **85**, 144428 (2012).